

# Preparation and Characterisation of Magnesium Oxide Doped Hydroxyapatite Derived from Eggshell Waste



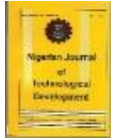
A. O. Ogunsanya<sup>1\*</sup>, E. O. Makinde<sup>1</sup>, A. F. Aba<sup>1</sup>, D. O. Daramola<sup>1</sup>, A. T. Olabinjo<sup>2</sup>, O. E. Ogundoyin<sup>3</sup>, K. A. Lawal<sup>4</sup>

<sup>1</sup>Department of Biomedical Engineering, Bells University of Technology, Ota, Nigeria.

<sup>2</sup>Department of Biological Sciences, Bells University of Technology, Ota, Nigeria.

<sup>3</sup>Department of Metallurgical & Materials Engineering, University of Lagos, Nigeria.

<sup>4</sup>Central Teaching and Research Laboratory, Bells University of Technology, Ota, Nigeria



**ABSTRACT:** Developing optimum biomaterials with enhanced regeneration process necessary for the proper bone tissue healing process is highly important. Hydroxyapatite is one of the most popular bioceramic due to its suitable biocompatible characteristics and similar native apatite of the human bone. Despite these attributes, hydroxyapatite has shortcomings related to its mechanical properties and bioactivation, which can be solved by composting or substituting with cation and anion of trace elements. In this study, hydroxyapatite and MgO-doped hydroxyapatite were prepared from biosources eggshell in a cost-effective and eco-friendly route (via combined wet hydrothermal, and co-precipitation techniques), aligning with the global trend towards circular economic and waste management. Samples were characterized by the physicochemical techniques, thermal stability, and bacterial and fungi growth using the pour plate technique. Results showed phase purity and features of hydroxyapatite, and the doped hydroxyapatite having shifted phase structure. Surface morphology showed fractured and interconnected pores good for cell proliferation. The particle size of 7.8 and 4.27  $\mu\text{m}$ , the percent porosity of 33.95 and 16.79 %, and the crystallinity of 29.99 and 40.04 %, respectively, were obtained. Both products showed good thermal stability up to 900 °C and no presence of microbial organisms was seen, revealing their biological properties.

**KEYWORDS:** Biomaterial, hydroxyapatite, hydrothermal, mechanical property, thermal stability

[Received Nov. 24, 2024; Revised Dec. 15, 2024; Accepted Dec. 26, 2024]

Print ISSN: 0189-9546 | Online ISSN: 2437-2110

## I. INTRODUCTION

In the last two decades, biomaterials have advanced significantly as a possible alternative in bone-tissue engineering applications (Dec *et al.*, 2022; Lee *et al.*, 2022). They can serve as a template in the implantation of cells and growth factors, act as an extracellular matrix to support the formation of new tissue and preserve tissue function to ensure optimal integration and regeneration. External roughness, porosity, pore size, interconnectivity of pore, degradation rate, mechanical properties, biocompatibility, and bioactivity are important properties for biomaterials to be considered in bone scaffolds (Etinosa *et al.*, 2024; Osuchukwu *et al.*, 2023; Osuchukwu *et al.*, 2022a; Osuchukwu *et al.*, 2022b; Perić Kačarević *et al.*, 2020) and design of smart biomaterials (Dauda *et al.*, 2021). Moreover, biomaterial should decompose into non-toxic components without causing any inflammatory effects (Krishani *et al.*, 2023; Perić Kačarević *et al.*, 2020).

Human bone is comprised mainly of organic (30%) and inorganic minerals (70%). These provide stiffness, proper mechanical properties, and remarkable regenerative ability (Zhang *et al.*, 2020). However, the ability for self-repair depends largely on the magnitude of the damage or the presence of a specific disease (Walmsley *et al.*, 2016). In

medical practice, bone abnormalities and their treatment have increased exponentially due to the severity or critical-size segmental bone defects resulting from traffic accidents, old age, non-union fractures, bone tumor removal, and others. Furthermore, defects occurring as a result of anomaly or injury of the anatomical or physiological composition have become a major clinical challenge in orthopedics and dentals compromising health and quality of life (Alonzo *et al.*, 2021). Autologous grafting has been the most preferred method of bone treatment because of histocompatibility and non-immunogenicity, with proven enhanced osteoinduction, osteogenesis, and osteoconduction. These factors have made standard grafting a popular substitute in bone transplantation (Sohn & Oh, 2019). However, recurrent deterioration, severe donor site damage, complications, malformations, and wounds, along with blood loss, swelling, and extensive expense. An increase in spinal fusion, joint fusion, and repair operations leading to a relative shortage of donors, has limited their use (Sohn & Oh, 2019).

Bone tissue engineering has become a key technological factor to facilitate the repair of damaged and diseased bone tissue. Biomaterials like metals, natural and synthetic polymers, ceramics, and their composites have been studied and used in bone tissue engineering (Qu *et al.*, 2019). Over the

\*Corresponding author: aogunsanya@bellsuniversity.edu.ng

years, researchers have concentrated on developing the best biomaterials for the improvement of bioactivity, the process of healing, and regeneration in osseous tissues. However, there is a major issue in difficulty generating an apatite layer comparable to human tissue (Stella *et al.*, 2022).

Hydroxyapatite (HAp), a versatile bioceramic, derived from natural and synthetic methods, has garnered significant attention because of its similarity to the native apatite of the human bone. Moreover, HAp possesses a high degree of biocompatibility, bioactivity, improved immune response, and osteoconductive, and osteoinductive properties (Etinosa *et al.*, 2024; Radulescu *et al.*, 2023). Sol-gel (Panda *et al.*, 2021), precipitation (Yelten-Yilmaz & Yilmaz, 2018), hydrothermal (Szterner & Biernat, 2022), microwave-assisted (Irfan *et al.*, 2021), and mechanochemical (Achar *et al.*, 2017; Mohd Pu'ad *et al.*, 2020) fabrication techniques have been used to produce HAp. The hydrothermal method is the most popular for synthesizing HAp nanoparticles due to its ability to form complex oxide powders with high crystallinity (Ebrahimi *et al.*, 2021). However, HAp (synthetic techniques) possess shortcomings regarding its mechanical properties such as brittleness, low fracture toughness (Goyal *et al.*, 2024), and bioactivation, which need to be improved upon to find importance in load-bearing applications (Mahanty & Shikha, 2021). In addition, due to the need for ultra-high characteristics, chemical components in synthetic HAp lack some important trace elements, some of which are expensive raw materials. Another major issue is the development of infectious microorganisms' material in bone growth and biological functions. One way to solve this problem is by composting with polymer and/or doping with trace elements like  $\text{Na}^+$ ,  $\text{K}^+$ ,  $\text{Mg}^{2+}$ ,  $\text{Sr}^{2+}$ ,  $\text{Zn}^{2+}$ ,  $\text{Fe}^{2+}$ ,  $\text{Ag}^+$ ,  $\text{Ce}^+$ ,  $\text{Ti}^+$ ,  $\text{Co}^+$ ,  $\text{Zr}^+$ ,  $\text{V}^+$ , and  $\text{Al}_3^+$ , or anions like  $\text{F}^-$ ,  $\text{Cl}^-$ ,  $\text{SO}_4^{2-}$ , and  $\text{CO}_3^{2-}$  (Asadipour *et al.*, 2019) or oxides of this element to improve its mechanical properties and bioactivity (George Ittycheria *et al.*, 2024; Radulescu *et al.*, 2023). Studies have focused on improving the properties of HAp using different doping agents and techniques. Natural resources have been used by different studies to fabricate HAp and doped HAp from seashells, eggshells, animal bones, fish bones (Etinosa *et al.*, 2024), and biological plants. Synthesizing HAp from natural resources allows bone regeneration to occur without implant failure. The production methods and the morphological control of HAp powders have been the subject of extensive research. Pure HAp has demonstrated bioactive features and poor mechanical properties. Therefore, the goal of the synthesis approaches should be to improve the poor mechanical properties of HAp (Osuchukwu *et al.*, 2023).

Karunakaran *et al.* (2020) developed magnesium (Mg)-doped mesoporous hydroxyapatite (HAp) nano-rods from seashell bio-wastes using a polyvinylpyrrolidone-assisted microwave technique. Findings from their study reveal similar morphology of mesoporous nano-rods, large specific surface area, pore diameters, and non-toxic, and potent antibacterial activity for biomedical implants when compared to pure HAP. In the study by (Predoi *et al.*, 2020), magnesium-doped hydroxyapatite was explored as a coating material. In another study by (Raafat *et al.*, 2020), Mg-doped HAp was synthesized as a cementing material in the production of biodegradable

porous nano-composite bone scaffolds using acacia gum and gelatin as the base polymers via a wet chemical method. Findings revealed nano-scale, improved mechanical properties, scaffold porosity of 26 – 39 %, bone-like apatite layer formation, and antibacterial properties. Mg-HAp nano-composite has a potential biomedical application in dental, orthopedic, and stem cell research (Jenifer *et al.*, 2021).

Using the solution combustion route, Obada *et al.* (2021) looked at the solution combustion route effect on strontium (Sr) doped hydroxyapatite (HAp). Their work revealed higher hardness and fracture toughness, and stability in phosphate buffer saline solution. Zhang *et al.* (2023) provide a thorough analysis of the Mg-nHA synthesis techniques and their use in biomedical applications. They outlined the benefits and drawbacks of Mg-nHA synthesis methods as well as some potential future developments. Their review methodically introduces the newest technologies for making Mg-nHA that are homogeneous, continuous, and have a range of morphological variations. It also gives us a look into a new area of research on bioactive materials that have new functions. (Mahanty & Shikha, 2024) investigated the effects of doping HAp with  $\text{Ag}^+$ ,  $\text{Mg}^{2+}$ , and  $\text{Zn}^{2+}$  ions on its microstructure, physiochemical properties, and mechanical properties via a sol-gel wet chemical route for use as a hard tissue implant. Their study reported reduced pore size, and surface area, increased mechanical property, reduced corrosion, enhanced wettability, and moderate thrombogenicity. Using the microwave-assisted hydrothermal technique, (Alanis-Gómez *et al.*, 2024) reported the successful incorporation of magnesium, producing high-purity, crystalline nanofibers with hexagonal morphology. Findings from their study demonstrate that HAp-Mg nanofibers are highly advantageous as biomaterials used in medicine, especially in reducing pathogens associated with implants and promoting additional clinical research. Bhatnagar *et al.* (2024) explored the incorporation of varying magnesium (Mg) contents to improve the structural and mechanical properties of HAp using the hydrothermal method and analyzed using theoretical simulations and experimental techniques. Their study stresses the osteogenic potential of HAp containing Mg and their oxides. Magnesium ( $\text{Mg}^{2+}$ ) ions have consistently replaced calcium in the chemical makeup of HAp. Although pure HAp exhibits weaker osteoblast adherence than  $\text{Mg}^{2+}$ , and large amounts may decrease cell adhesion (Mustafa *et al.*, 2020).  $\text{Mg}^{2+}$  and their oxides are important elements of bone mineral, homeostasis, bone cell function, and differentiation of stem cells into osteoblasts (Ciosek *et al.*, 2021; Hung *et al.*, 2019). Moreover, they have similar density and elasticity values with bone, making them a promising option for medical implants due to their biocompatibility and their good antimicrobial properties against gram-positive and gram-negative bacterial (Haghshenas, 2017; Predoi *et al.*, 2019; Raveendran *et al.*, 2013). These attributes make them a suitable choice for doping in HAp.

From the literature, limited studies has been conducted on MgO particles as dopant in HAp. In addition, majority of the studies conducted were  $\text{Mg}^{2+}$  metal alloy substituted synthetic HAp. Studies on using MgO particles as a doping agent in natural-based derived HAp need to be explored further. It is on

this basis the idea of examining eggshell-derived HAp and MgO doped eggshell-derived HAp samples formed as a first step in assessing its potential use as an implant material. Furthermore, the necessity of fabrication technology of HAp and doped HAp from biosources waste material that is cost-effective, simple, and safe becomes imperative. The present study focuses on the preparation and characterization of synthesis of HAp and MgO-doped HAp from eggshell wastes utilizing hydrothermal and co-precipitation techniques, using eggshell wastes as the precursor of HAp. The objective of this study is to prepare and assess the physiochemical and thermal properties of eggshell-based HAp, and MgO-doped eggshell-based HAp for enhanced mechanical and bioactivity properties. HAp was synthesized by combining techniques (wet chemical and hydrothermal calcination) and doping of synthesized HAp by variation of magnesium oxide (MgO) via co-precipitation technique. The synthesized HAp and doped HAp can serve as bone substitute materials, orthopedic and dental implants, coating on implants, and other biomedical applications (Das Lala *et al.*, 2021). The present paper aims to contribute to the sustainable material to aid research in the field of bone tissue engineering.

## II. EXPERIMENTAL METHODOLOGY

### A. Material Preparation

Brown eggshell waste (1000 g of lumps) was obtained from the local food vendor at Bells University of Technology, Ota, Nigeria. The raw eggshell was cleaned, dried in an oven, and then ground to remove flesh, lipids, membrane, or other clinging materials. Eggshell lumps were washed with distilled water five times to get rid of dirt, boiled for 2 hours to remove dirt and membrane attachment further, and left to dry in the air for 24 hours. The dried eggshell was washed again using distilled water three times and then dried in the laboratory environment for 24 hours further before being oven dried at 105 °C for 6 hours. Dried eggshell particles were ground using mortar and pestle and sieved using a mechanical sieve shaker to obtain particle size (900 µm). Magnesium oxide (MgO) purchased from TUNNEX laboratory material served as the doping material in particle form. Table 1 shows the composition of the MgO filler material as received in analytical grade type. The loss-on-ignition on the doping material was carried out to remove the volatilized materials. Briefly, 5.01 g of sieved powders of MgO were used (>900 µm). The wet sample was weighed as a wet weight in a crucible and then oven-dried at 105 °C in a UNISCOPE laboratory oven for 6 hours before being heat-treated in a muffle furnace at 600 °C for 2 hours (Ogunsanya *et al.*, 2024).

Table 1. Composition of the MgO filler

Percentage Composition	% Mg	% Cl	% Fe	% SO <sub>4</sub>	% Others
MgO	99.25	0.15	0.1	0.5	<0.001

### B. Sample Preparation

In this paper, the natural hydroxyapatite (HAp) was synthesized from an eco-friendly biowaste agricultural material source (eggshell powder) via hydrothermal wet precipitate following the stated approach. 611 g sieved eggshell powder lumps were calcined at 700 °C for 2 hours at a heating rate of 15 °C/minute to remove decomposed carbonates as revealed in chemical equation 1 (Ogunsanya *et al.*, 2024).



Then, an equal weight volume of calcium oxide and distilled water was prepared and stirred for 2 hours using a magnetic stirrer as revealed in chemical equation 2. 1000 ml of an equal volume of disodium hydrogen orthophosphate and potassium dihydrogen orthophosphate was prepared, and then, added drop-wise to the solution sample, stirred for 2 hours further, and then heated for 1 hour at 50 °C in a hot air oven (low-temperature sintering). The sample was then washed with distilled water and filtered, maintaining a neutral pH. Samples were oven dried for 24 hours at 80 °C and further grounded using mortar and pestle to obtain a grayish-white natural HAp dry powder. Figure 1 revealed the flow chart of the production of hydroxyapatite and doped samples from eggshell lumps.



20 g of the grayish-white HAp powder was dissolved in 75 ml of distilled water and stirred for 2 hours to form a solution. After stirring, a solution of 0.6 molar of conc. Phosphoric acid (98 % purity) was prepared and then, added to the solution in a drop-wise manner. Afterward, the samples were further stirred for 2 hours, covered with aluminum foil, and allowed to age for 48 hours. After aging, to eliminate any contaminants, the solution was further washed with deionized water and distilled water. The solutions were heated for 4 hours at 105 °C in a prepared oven, cooled at room temperature, and then ground into powdery form using mortar and pestle to increase the surface area. The ground sample was calcined at 700 °C for 4 hours using a muffle furnace. Samples were left to cool in the muffle furnace and then, sieved upon cooling to obtain the produced hydroxyapatite powder.

In the case of the doped HAp, the same approach of wet hydrothermal synthesis produced grayish white powder HAp was employed using the co-precipitate technique. Percent weight of the magnesium oxide (MgO) was added at variable weighted samples of the produced grayish HAp powder and 75 ml of deionized water as shown in Table 2. The solution was stirred for 2 hours, then drop-wise addition of the prepared

concentrated phosphoric acid, before being aged for 48 hours. The solution was washed with deionized water and distilled water to get rid of contaminants, oven-dried for 4 hours at 105 °C, and then allowed to cool at room temperature. Grinding of cooled samples into powdery form using mortar and pestle to increase the surface area, followed by calcination at 700 °C for 4 hours and then sieving upon cooling to obtain white hydroxyapatite powder. The percentage residue and yield was determined using Equation 3 and 4.

$$\text{Percentage Residue} = \frac{M_1 - M_2}{M_1} \times 100 \quad (3)$$

$$\text{Percentage Yield} = \frac{M_2}{M_1} \times 100 \quad (4)$$

Where  $M_1$  is the initial mass of samples before calcination and  $M_2$  is the final mass of samples after calcination.

Table 2. Batch formation of doped HAp structure

Sample	Produced HAp [g]	MgO [g]	Distilled Water [ml]
A	17.5	2.5	75
B	15.0	5.0	75
C	12.5	7.5	75

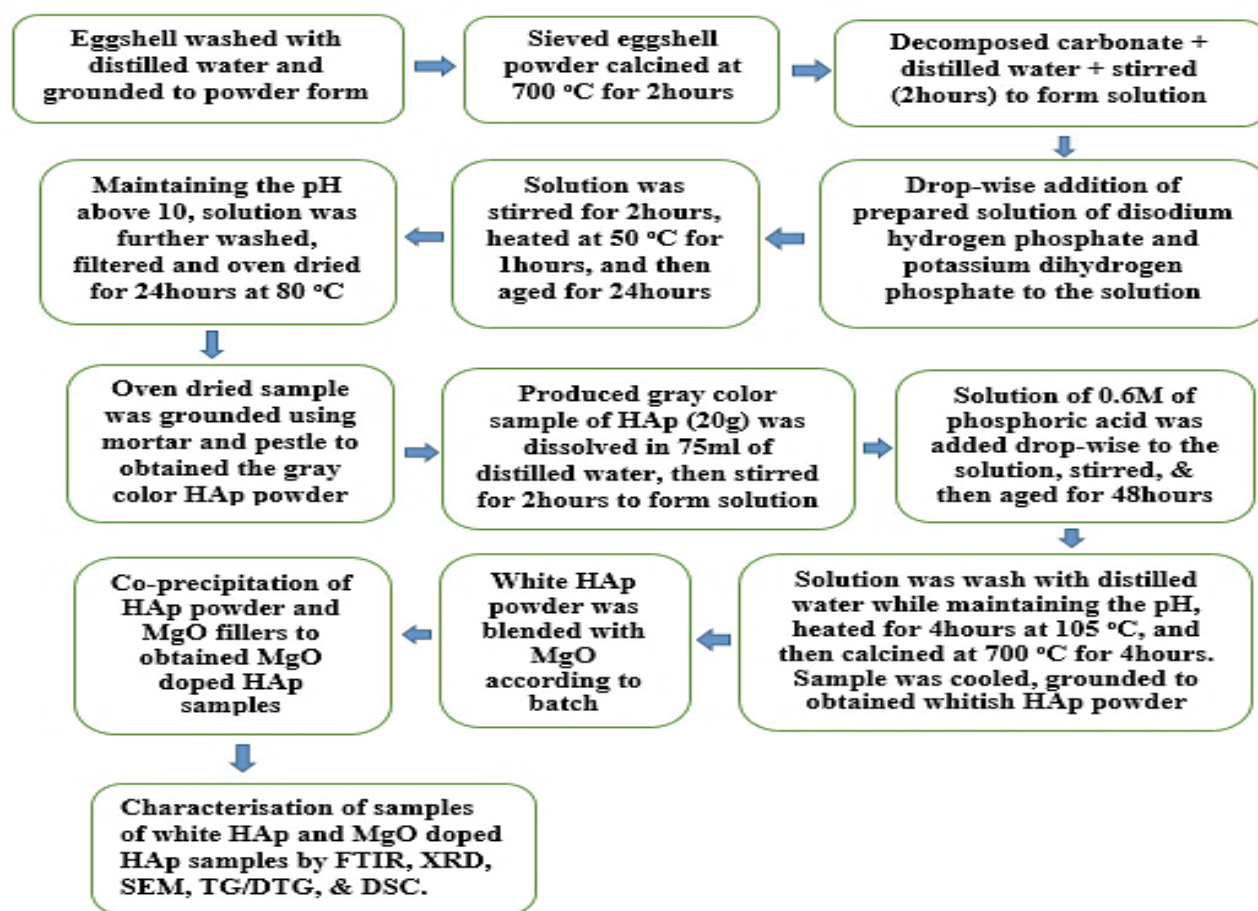


Figure 1. Flow chart of preparation of HAp and doped HAp structure

### C. Phase and Morphological Characterization of Samples

The infrared absorption spectra to identify the functional groups present in the HAp and doped Hap, and to assess the variations in the reported spectra to indicate the existence, emergence, or potential extinction was obtained by Fourier Transform Infrared Spectroscopy (FTIR) technique (Perkin-Elmer 3000 MX spectrometer model). All spectra were recorded in attenuated total reflectance (ATR) mode over a

wavelength of 4000 to 450  $\text{cm}^{-1}$  and 32 per scan spectrum using a resolution of 4  $\text{cm}^{-1}$  along with a peak sensitivity of 2  $\text{cm}^{-1}$ . The crystalline structure and crystal properties were investigated by X-ray diffraction technique (XRD). Each sample was run through the Rigaku SmartLab Diffractometer (Rigaku Int. Corp. Tokyo, Japan) at a diffraction scanning rate of 2 °/min within the 2 to 50° at room temperature with CuK $\alpha$  radiation set at 40 kV and 40 mA. Data was collected and analyzed using OriginPro Software. For phase identification,

the spectrum of the obtained HAp and HAp were validated against the XRD pattern of HAp (International Center for Diffraction Data (ICDD) standard: (JCPDS 21-1276), (JCPDS 21-1272) and (JCPDS 09-432)). Percentage crystallinity was calculated using equation 5.

$$\frac{\text{Area of Crystalline Peaks}}{\text{Area of Crystalline Peaks} + \text{Area of Amorphous Peaks}} \times 100\% \quad (5)$$

The surface morphological structure of the outer surface of the image was examined using the Scanning electron microscope (SEM) (GEMINI Ultra 55), which also provided immediate details regarding the typical size and shape of the acquired HAp and doped HAp. The samples were fixed on carbon tape and dried overnight. Electrically conducting material was coated on the samples.

#### D. Thermal Characterization of Samples

Thermogravimetric analysis (TGA) was used to evaluate the decomposition rate of the samples. A weight of approximately 12.6 mg of each sample was used for the analysis. Some of the material was used to coat the bottom of the pan. An investigative scan conducted at 10 °C to 20 °C per minute started and ended at 900 °C below the transitional point of the samples. The survey scan was then evaluated, and the start and finish temperatures were changed as appropriate. Differential thermal analysis (DTA) was used to analyze the samples using PerkinElmer DTA. The samples are heated or cooled alongside a neutral reference, under the same conditions. Any temperature variance in the sample and neutral reference was noted and documented. Differential scanning calorimetry (DSC) analysis was carried out to examine the thermal properties of the samples further. 3.70 mg of the HAp and 3.20 mg of the doped HAp samples were used for the analysis. The sample was measured in a DSC pan and then placed in the DSC calorimeter alongside an empty pan, which was used as a reference. Afterward, the calorimeter was programmed to control the temperature range. The sample was then heated and cooled. The temperature and heat flow difference data was collected and plotted as a DSC curve.

#### E. Bacterial and Fungi Growth Analysis

In this study, the presence of bacterial and fungi growth effects on the samples was tested using SSA, EMB Agar, MacConkey Agar, PDA, BAB, and Nutrient Agar, respectively. The Pour plate technique was used in bacterial and fungi growth effect analysis, which involves the introduction of the samples before the addition of the agar. The technique involves the preparation of Peptone solution by dissolving 5.5 g of Peptone powder in 220 ml and then sterilizing it in a manual autoclave machine at 121 °C for 15 minutes. Also, to prepare the agar solution, the required agars were dissolved in 250 ml of distilled water and sterilized after the complete sterilization of the peptone water. Then, petri dishes were sterilized in a hot air oven at 160 °C for 2 hours. After that, the dishes were removed from the hot air oven and, placed in the Laminar flow machine with UV light for 15 – 30 minutes to sterilize the dishes further. Then, 1 g samples of HAp and doped HAp were introduced into 9 ml of peptone solution (weight/volume) and after dissolving, 1 ml of the dissolved samples were plated in the Petri dish before the introduction of the required agar solutions into the Petri dishes containing the solution. Samples were incubated at 37 °C except for the samples with the PDA solution which needed to be at room temperature.

### III. EXPERIMENTAL RESULTS ANALYSIS

#### A. Material Formation

The colors obtained could be a result of the quantity of organic substances removed from the eggshell during the fabrication process. A clear difference that was observed from the eggshell powder was the changing of brownish color of the eggshell to grayish-white color after the first step of calcination at 700 °C for 2 hours indicating the breakdown of the calcium carbonate into calcium oxide and release of carbon dioxide as seen in equation 1. However, after varying hydrothermal wet precipitation, there was a distinct difference in the color of the samples (grayish color obtained in the first step calcination to white after second step calcination) to form the hydroxyapatite powder. This variation is potentially linked to the inference about organic substances. Table 3 shows the mass of samples before and after calcination, along with the percentage residue, percentage yields, and mass loss (100% - %Y) using equation 3 and 4, respectively.

Table 3. Percentage residue, percentage yield, and mass loss of HAp and doped HAp sample

Sample	Mass of Sample Before Calcination [g]	Mass of Sample After Calcination [g]	Percentage Residue [%]	Percentage Yield [%Y]	Mass Loss [100% - %Y]
Control HAp	20	16.16	19.20	80.8	19.2
Batch1 (17.5HAp/2.5MgO)	20	17.13	14.35	85.65	14.35
Batch2 (15HAp/5.0MgO)	20	16.36	18.20	81.8	18.2
Batch3 (12.5HAp/7.5MgO)	20	19.30	3.50	96.5	3.5

### B. FTIR Analysis

Figure 2 represents the absorption spectra plot of the synthesized HAp and MgO doped HAp calcined at 700 °C as a result of the similarity in the spectra. Based on the absorption spectra, the chemical performance of the synthesized samples

was examined, and two distinctive regions (fingerprint region (1500 – 500  $\text{cm}^{-1}$ ) and functional group region (1500 – 4500  $\text{cm}^{-1}$ )) were represented in the plot (Ogunsanya *et al.*, 2024). The vibration characteristic bands of hydroxyapatite were observed that is O-H,  $\text{CO}_3$ ,  $\text{PO}_4$ , and  $\text{H}_2\text{O}$ .

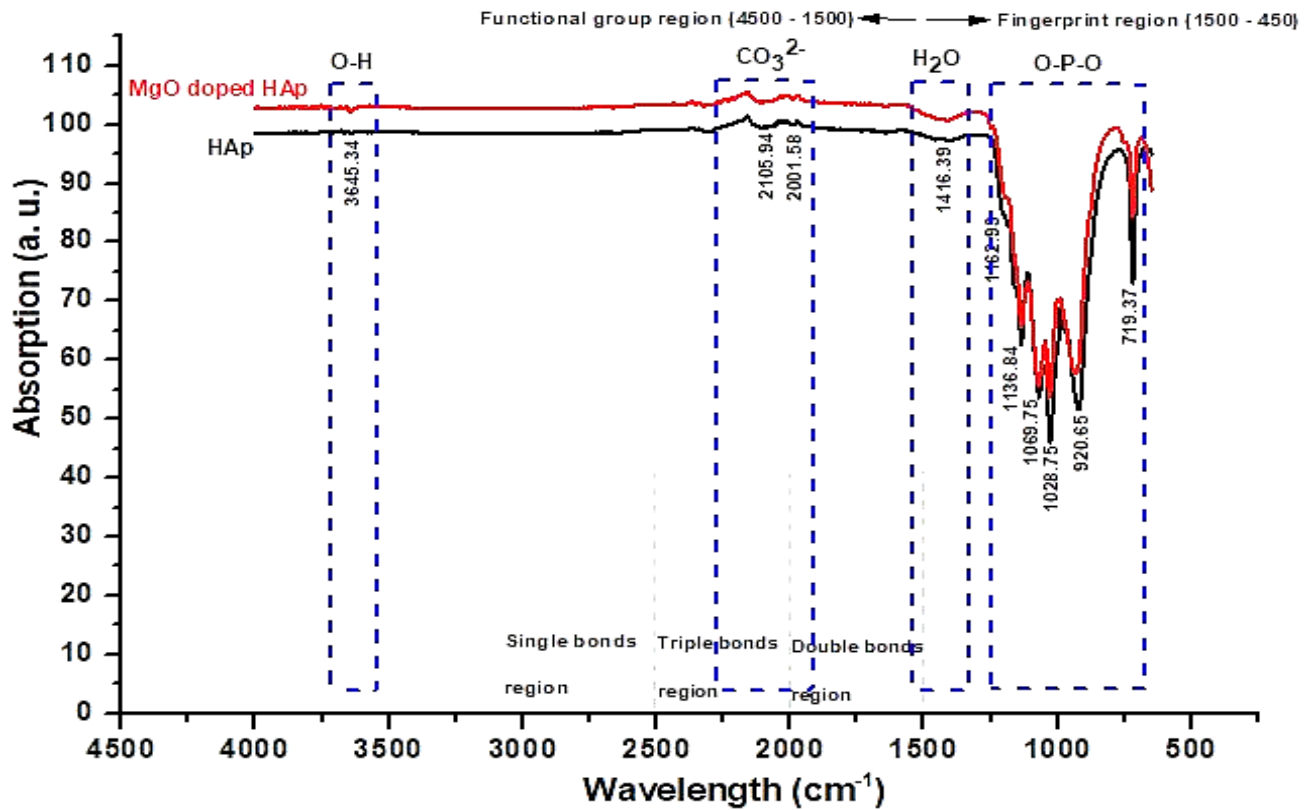


Figure 2. FTIR plot of the HAp and MgO doped HAp Sample

### C. X-ray Diffraction Analysis

Figure 3 shows the crystal phase plot of the synthesized HAp and MgO-doped HAp, respectively. The diffraction peaks observed can be indexed to planes (001) (0 0 2) (1 1 0)

(2 1 1) (3 0 0) (2 0 2) (1 0 1) (0 0 4) (2 1 2) (2 1 1) (2 2 0) (2 0 4) (1 1 1) (2 2 2) and (2 2 0) are strongly consistent with those of International Center for Diffraction Data spectrum: (JCPDS 21-1276), (JCPDS 21-1272) and (JCPDS 09-432) standard HAp.

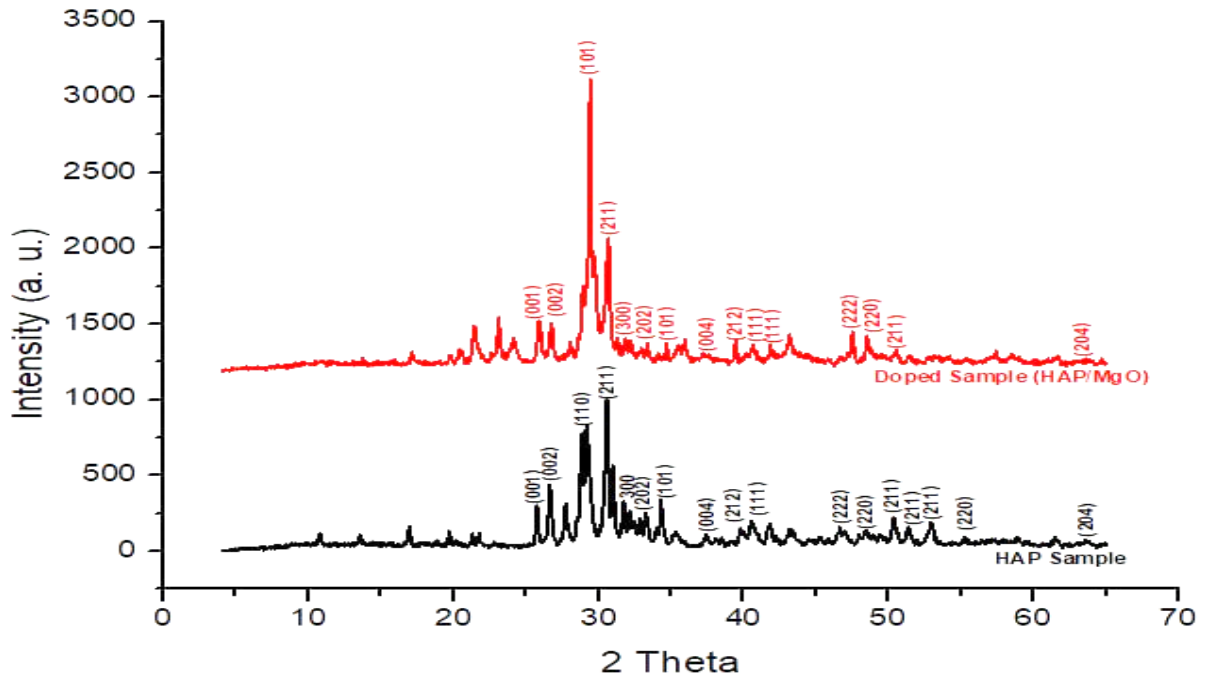
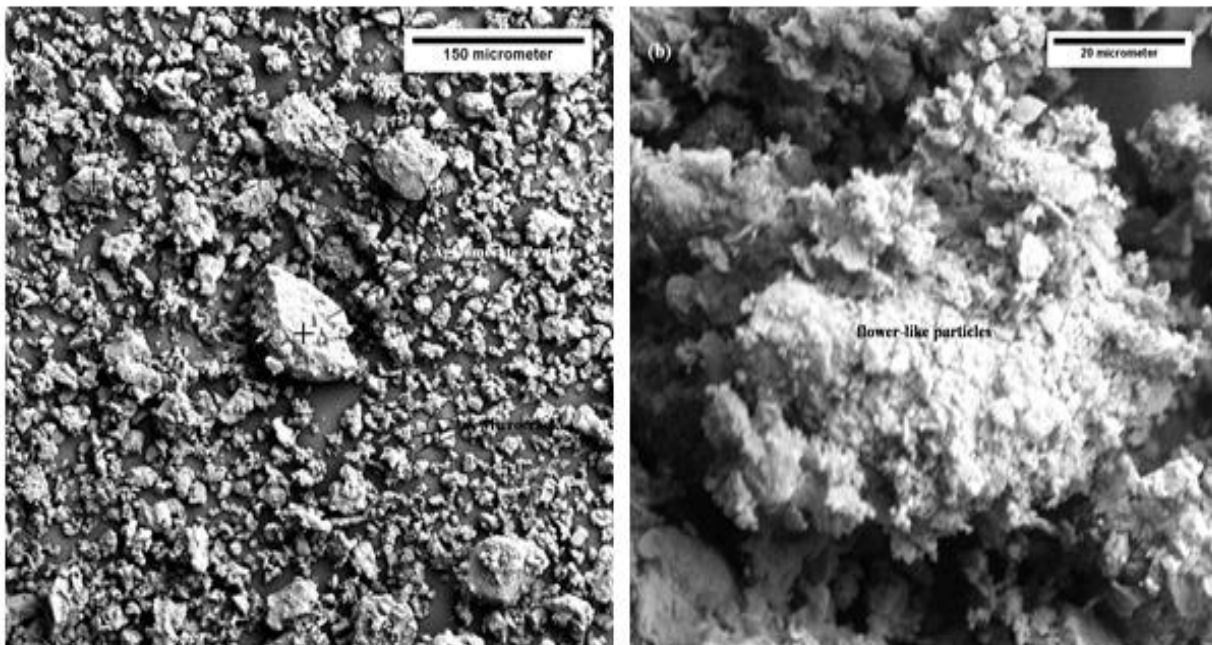


Figure 3. XRD patterns analysis of synthesized Natural based HAp and Mg/Doped HAp composite

#### D. Morphological Phase Analysis

Figure 4 shows the SEM image of the samples at a magnification of 2000X. The produced HAp exhibits an almost uniform spherical, non-homogenous, irregular agglomerated

structure as shown in Figure 7(a). The external surface of the MgO-doped HAP shows finer and uniform flower-like particles as shown in Figure 7(b).



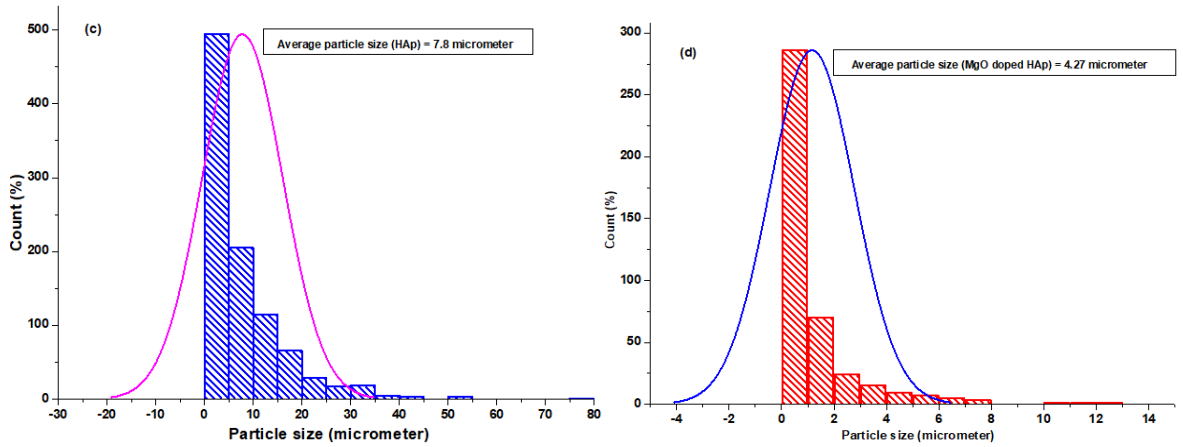


Figure 4. SEM analysis of the (a) hydroxyapatite and (b) MgO doped hydroxyapatite samples synthesized at 700°C (c) particle size distribution of HAp (d) particle size distribution of MgO doped HAp

E. Thermal Stability Analysis

Thermogravimetric (TG) and heat flux curves of the synthesized HAp sample are depicted in Figure 5 from 30 – 850 °C. Three inflection points were observed in the eggshell-

based HAp powder at 150, 462, and 707.56 °C, and four thermal events (mass losses).

Figure 6 shows the TG/DTG curve of the MgO-doped HAp sample with two inflection points and three thermal events.

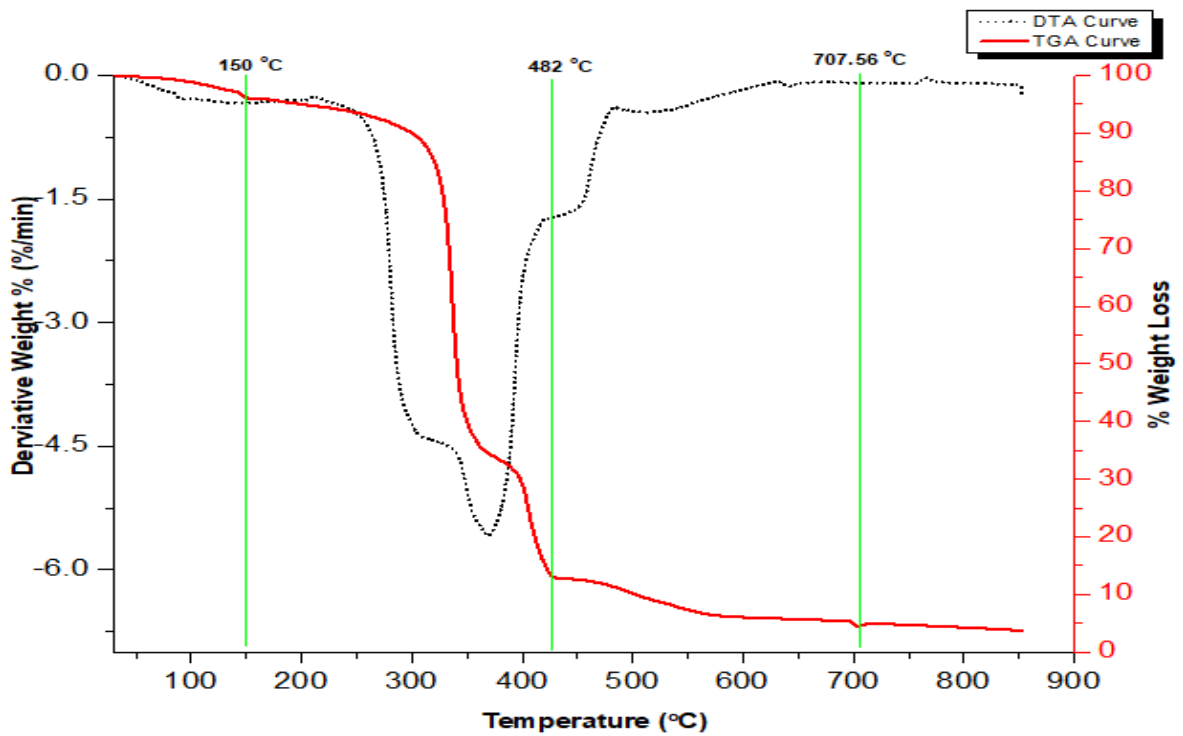


Figure 5. TGA and the corresponding DTG of synthesized Natural Based HAp

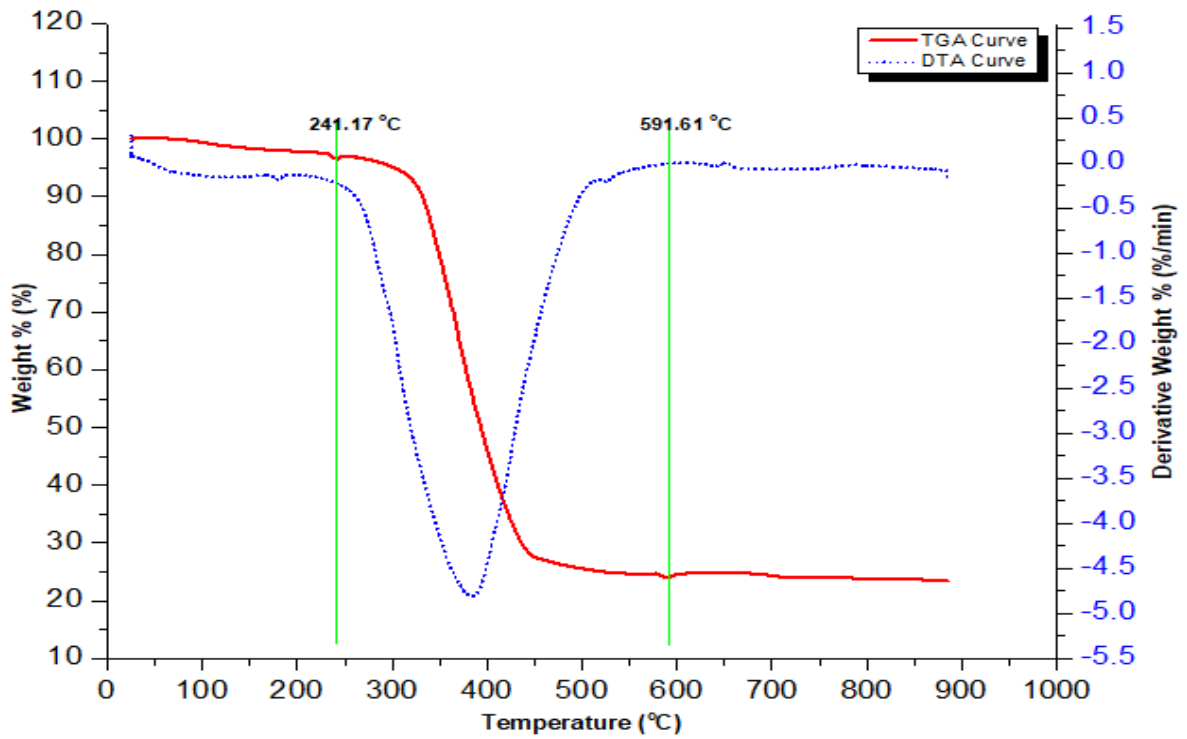


Figure 6. TGA and the corresponding DTG of synthesized MgO doped HAp

Figure 7 shows the DSC analysis of the synthesized natural-based HAp and MgO-doped HAp with the heat flow

(mW/mg). The DSC curve depicts both endothermic and exothermic characteristics, and baseline shifted.

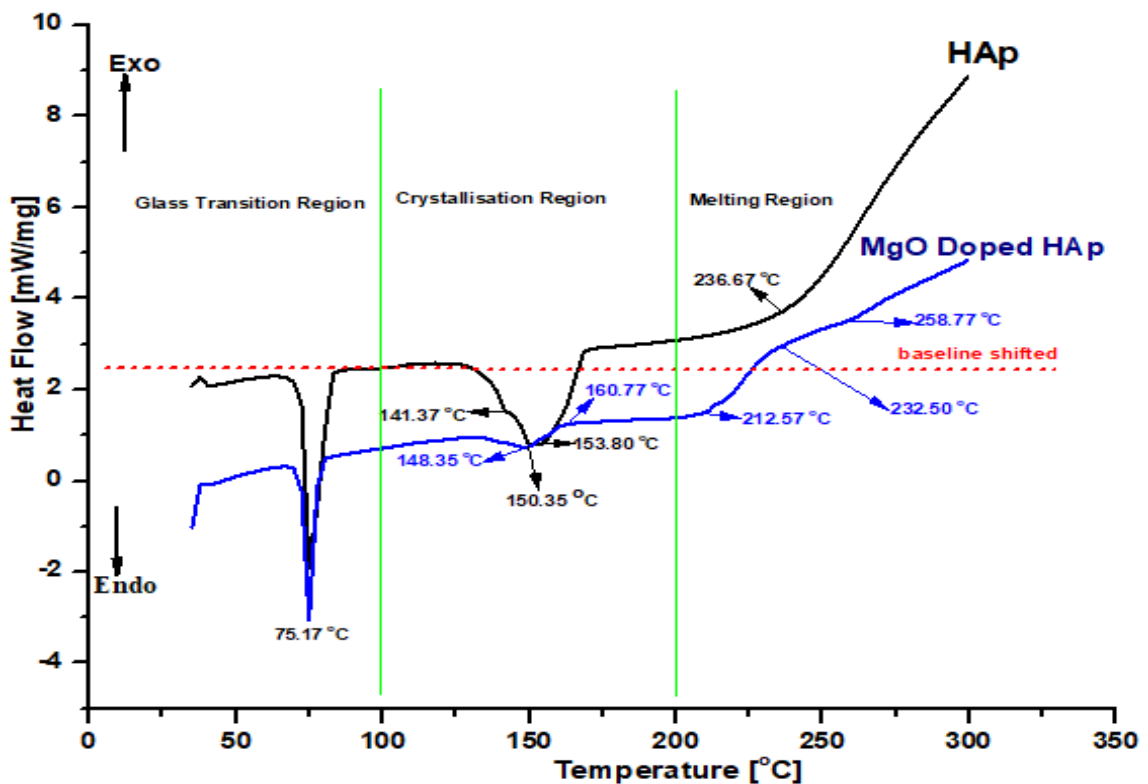


Figure 7. DSC analysis of synthesized natural-based HAp and MgO-doped HAp

### F. Analysis of Bacterial Growth Effect

Table 4 shows the bacteria and fungi used in the analysis of samples, along with their corresponding weight and volume

of distilled water. Samples were plated for 24, 48, and 72 hours to collect bacterial and fungi growth effects.

Table 4. The weight of agars used and bacteria tested

Agars used	Weight per 1000ml distilled water [g]	Weight per 250 ml distilled water [g]	Bacteria tested	Growth Effect
MSA	111.02	27.8	Staphylococcus aureus	No growth
EMB	35.96	9.0	E. coli	No growth
SSA	63.02	15.8	Salmonella and shigella	No growth
MacCONK EY	50	12.5	Total coliform	No growth
PDA	39	9.8	Mold and yeast	No growth
BAB	37	9.3	Faecal streptococci	No growth
Nutrient	28	7.0	Total plate count	No growth

## IV. DISCUSSION

In the present study, we prepared and accessed the physicochemical and thermal stability of HAp eggshell-based material and MgO-doped HAp material prepared via combined hydrothermal and co-precipitation techniques as potential scaffold material in bone tissue engineering applications (Ogunsanya *et al.*, 2024). The prepared HAp and doped samples were assessed further for antibacterial properties using the pour plate technique. Eggshell waste was used in the study due to its usefulness in bone tissue engineering applications and its potential as raw material for producing hydroxyapatite, an important element present in the bones and teeth. Biogenic hydroxyapatite has been a proven material utilized in bone repair and tissue regeneration with low treatment costs and minimal environmental impact (Asmawati, 2017). Different materials and fabrication techniques have been used to prepare HAp. Meanwhile, the hydrothermal technique has been studied in producing porous and nanoparticle material because of complex oxide powder formation and high crystallinity. The prepared samples were assessed by FTIR, XRD, SEM, TGA, DTA, and DSC. Choosing appropriate materials for bioceramic composite is very crucial in bone tissue regeneration.

The material formation of the brownish eggshell particles showed grayish-white colors after the initial phase of calcination at a temperature of 700 °C. This signifies the complete or partial elimination of organic matter from the unprocessed eggshell powder. The degree to which organic matter was eliminated from the original material during the calcination stage determines the color. Therefore, the subsequent stage of hydrothermal calcination at a comparable

temperature was necessary to get the appropriate white color of the HAp and doped HAp. It implies that simultaneous hydrothermal calcination was appropriate for eliminating organic matter from the unprocessed eggshell powder (Akindoyo *et al.*, 2019). Meanwhile, the mass of the samples reduces after the hydrothermal wet calcination and co-precipitation techniques, further, confirming the total removal of the organic matter with better yield (Table 3).

The functional group arising from the vibration characteristic bands of hydroxyapatite were observed, that is, O-H, CO<sub>3</sub>, PO<sub>4</sub>, and H<sub>2</sub>O (Figure 2). The phosphate group shows stretching symmetrical peaks of the phosphate group (PO<sub>4</sub><sup>3-</sup>), and degenerated asymmetrical vibration bands of the triply phosphate group at 719.37 and 920.65, and 972.82 cm<sup>-1</sup>, respectively. Meanwhile, the characteristics of symmetrical stretching of  $\nu_3$  (triply phosphate group (PO<sub>4</sub><sup>3-</sup>)) were at 1028.75 and 1069.75 cm<sup>-1</sup>, respectively. The maxima spectra domains of 1136.84 cm<sup>-1</sup> revealed symmetrical stretching of  $\nu_4$  of the phosphate group, and asymmetrical stretching appears at 1162.93 and 1189.02 cm<sup>-1</sup>. A broad vibration bending band at 1416.39 cm<sup>-1</sup> could be ascribed to the water molecules. The carbonate phase appears at 2105.94 and 2001.39 cm<sup>-1</sup>, respectively, with bending vibration bands. This comes from type A carbonate replacement, suggesting the existence of a surface -CO<sub>3</sub><sup>2-</sup>. The presence of hydroxyl groups (from the HAp structure) at 3599.17 cm<sup>-1</sup>, adsorption of molecules of water, and the distinctive vibration of phosphate were the leading causes of the prevailing maxima seen in the FTIR spectra which is in agreement with literature reports (Predoi *et al.*, 2023).

After doping the synthesized HAp samples, the phosphate group shows stretching symmetrical and

degenerated asymmetrical vibration bands at 719.37, 931.83, and 998.93  $\text{cm}^{-1}$  (Figure 2). Meanwhile, the characteristics of symmetrical stretching of  $\nu_3$  and  $\nu_4$  were at 1032.47, 1073.47, and 1136.84  $\text{cm}^{-1}$ , respectively. Asymmetrical stretching of  $\nu_4$  was at 1196.48 and 1248.66  $\text{cm}^{-1}$ , respectively. The broad vibration bending band at 1416.39  $\text{cm}^{-1}$  ascribed to the water molecules was also seen. The carbonate phase appears at 1944.13 and 2109.67  $\text{cm}^{-1}$ , respectively, with bending vibration bands, meanwhile, the O-H appears at 3645.67  $\text{cm}^{-1}$ . A significant shift of wavelength was observed after doping the HAp samples, however, doping the HAp material with magnesium has led to a decrease in the intensity of the functional groups. In this study, biogenic hydroxyapatite from natural resources has been improved by doping with metal oxide ions substitute (MgO) to increase property, thereby, substituting the cations ( $\text{Ca}^{2+}$ ) and anion ( $\text{PO}_3^{4-}$ ) in hydroxyapatite with  $\text{Mg}^{2+}$  and  $\text{OH}^-$  of the dopant, this is in agreement with the literature of (Radulescu *et al.*, 2023). This substitution type asset hydroxyapatite bioactivation because the negative charge carriers are initiated, which can promote the bone-type apatite (Horta *et al.*, 2021).

The XRD diffraction peaks appear narrow, sharp, and very intense, indicating the samples' good crystalline properties (Figure 3). This suggests that the combined techniques were able to remove the organic matter from the raw eggshell powder without any changes to the molecular skeleton of the HAp product. The peaks at  $2\theta$  and  $4\theta \approx 27.7$ , 29.1, 30.1, 31.7, 41.7, 43.7, and 46.7 designate point that these peaks match the original XRD of HAp with the standard card number of JCPDS 0432-009 for the nanocrystalline hydroxyapatite (Sahmani *et al.*, 2019). The percentage crystallinity of the synthesized HAp and Mg-doped HAp was calculated to be 29.99 % and 40.04 %, respectively. An increase in the peak intensity indicates the introduction of  $\text{Mg}^{2+}$  ions which is in agreement with the literature (Jenifer *et al.*, 2021). This suggests that doping HAp with  $\text{Mg}^{2+}$  oxide resulted in increased crystallinity. MgO dopant led to an observable change in the lattice parameters, and possible replacement of larger groups, such as tetrahedral phosphates in the HAp sample with smaller groups, in this case, possibly planar carbonates. This indicates the substitution of the carbonate groups into the HAp. Thus, it is confirmed the  $\text{Mg}^{2+}$  ion present in the HAp causes the crystal structure to change, thereby, enhancing the HAp characteristics (Jenifer *et al.*, 2021).

The surface morphology and geometry of the scaffold are its critical components. The morphology of the produced HAp exhibits uniform spherical, non-homogenous, irregular agglomerated structure and shape, which could be attributed to the technique and conditions of synthesis, and one of such shapes reported is spherical (Pu'ad *et al.*, 2020), which is in good agreement with the observation from this study (Figure 4a). The average particle size distribution was 7.8  $\mu\text{m}$  with a percentage porosity of 33.95 %. The microcrack indicates the poor properties of the material, which can be attributed to the presence of the functional groups  $\text{Ca}^{2+}$ ,  $\text{OH}^-$ , and  $\text{PO}_3^{4-}$ . It is interesting to note that the techniques employed in this study revealed reasonable interconnectivity similar to natural bone apatites. The external surface of the MgO-doped HAp sample has finer and more uniform particles with flower-like

morphology (Figure 4b). This implies that the doped HAp has a surface area for cell proliferation (Liu *et al.*, 2020). The uniform distribution of particles has been reported to improve mechanical strength (Karacabey *et al.*, 2019). Compared to the synthesized eggshell natural-based HAp, the average particle size distribution, and percentage porosity were reduced to 4.27  $\mu\text{m}$  and 16.79 %. This represents a strong chance that doped HAp may crystallize and develop. The results of the XRD investigation are consistent with the growth of crystal sizes that have been observed. Thus, making the samples a good candidate biomaterial for bone tissue engineering applications.

The TG/DTG analysis of the produced HAp revealed inflection peaks and thermal events. The event that appears around  $<200^\circ\text{C}$  could be attributed to the loss of water molecules absorbed by the HAp material, and the event around  $200^\circ\text{C} - 428^\circ\text{C}$  is due to the loss of structural water as a result of the dehydration. The event that occurs from  $428^\circ\text{C}$  to  $707.56^\circ\text{C}$  corresponds to water strongly bonded (intracrystalline water). The last event was between  $707.56^\circ\text{C}$  and  $850^\circ\text{C}$  due to the decomposition of carbonate (Figure 5). The weight loss in the temperature range of  $100 - 150^\circ\text{C}$  indicates that the reaction is calcinated with phosphate (oxidation-reduction). Meanwhile, for the DTG curve, the thermal decomposition (endothermic peaks) appeared at 90.85, 211.99, 371.39, 484.03, 641.68, and 766.49  $^\circ\text{C}$ ; this peak is due to the degradation of residual water according to literature by (Bakr *et al.*, 2022; Canbay *et al.*, 2018). For the doped sample, two inflection points were observed at  $241.17^\circ\text{C}$  and  $591.61^\circ\text{C}$  with three thermal events (Figure 6). The event that occurs at  $<300^\circ\text{C}$  can be attributed to the removal of free water from the pores, with a further decrease in weight loss due to the removal of water. The event that happens between  $241.17^\circ\text{C}$  and  $591.61^\circ\text{C}$  is an indication of the dehydration of hydroxide. Meanwhile, the thermal event at  $591.61^\circ\text{C}$  and  $850^\circ\text{C}$  can be attributed to the decomposition of carbonate which is in agreement with the literature (Monte *et al.*, 2022). The thermal decomposition (endothermic peaks) occurs at  $100^\circ\text{C}$ ,  $181.43^\circ\text{C}$ ,  $380^\circ\text{C}$ ,  $527.87^\circ\text{C}$ ,  $651.34^\circ\text{C}$ , and  $792.80^\circ\text{C}$ , respectively, due to the degradation of residual water.

The DSC reported the occurrence of an endothermic peak at around  $75.17^\circ\text{C}$  (removal of water from the sample). The broad peak near  $141.37$  and  $153.80^\circ\text{C}$  represents the evaporation of absorbed and lattice water as a result of the heating (liberation of chemically bonded water). An endothermic peak occurs at  $236.67^\circ\text{C}$  which indicates the crystallization of the hydroxyapatite (HAp) at that temperature (Figure 7). This is in agreement with the results of the study on hydroxyapatite carried out by (Waheed *et al.*, 2015). For the MgO-substituted HAp sample, the filler caused a dramatic change in material structure. A new broad endothermic peak occurs at  $148.35^\circ\text{C}$  as a result of the loss of water molecules due to evaporation of absorbed and lattice water. This can be due to the melting of crystalline assigned structures. Furthermore, an endothermic mode that occurs at  $212.57$  and  $258.77^\circ\text{C}$  is indicative of the decomposition of the assigned structures or structure relaxation and filler assigned decomposition. This is similar to the findings of (Bulina *et al.*, 2024). The occurrence of a broad and more prominent endothermic peak in synthesized MgO doped HAp as

compared with the small and sharp endothermic peak in HAp (smaller stability of crystallites, and after adsorbed water elimination at 75.17 °C there were two steps at 141.37 and 150.35 °C to the relaxation process in different local structures). The incorporation of MgO into the structure of HAp to form MgO/HAp composite with less crystallinity that can be caused by a very small size of crystals obtained or due to the formation of metastable improves the thermal property of the material. Decomposition of MgO occurs at temperatures above 300 °C. The results of this work have provided information on the improvement of the physiochemical and thermal properties of HAp with magnesium oxide fillers. The filler decomposition shifts to the highest temperature.

The samples showed no sign of bacterial and fungi growth after 24, 48, and 72 hours of incubation (Table 4). This may be due to the sterility and the ability of the HAp and doped HAp to inhibit bacterial growth. The analysis of the pour plate technique provides insight into the potential antibacterial properties of the HAp material (Elmaazouzi *et al.*, 2024). The ability of the samples to inhibit bacterial growth further confirmed the anti-microbial abilities of the HAp and doped HAp. Doping of HAp has been used to create micro- and nanosized fibrous composites to replicate the natural extracellular matrix. For tissue engineering applications, nanofibrous biomaterials may be created to replicate the natural extracellular matrix (ECM). The osteoblast adhesion and proliferation could also be enhanced by surfaces that imitate the nanoscale shape of the bone surface. Moreover, compounds at the nanoscale can facilitate cell attachment and group together according to their patterns. Even in the absence of growth stimuli, the surface topography functions have an extracellular physical environment that enhances cell function (Mustafa *et al.*, 2020). The utilization of bioceramic materials such as HAp and doped HAp from biogenic natural resources eggshell powder for improved physiochemical, thermal, and mechanical properties, and osteoconductivity seems to be the most prospective bone substitute. Accordingly, this work supports environmental sustainability and encourages the use of natural debris like eggshells and MgO metallic oxide doped HAp in the manufacturing of valuable biocomposites, which aligns with the contemporary concepts of sustainable development applied to bone tissue regeneration.

## V. CONCLUSION

This study assesses the physiochemical, biological, and morphological properties and thermal stability of hydroxyapatite and MgO-doped hydroxyapatite synthesized from natural-based (eggshell) waste for bone tissue engineering experiments. The HAp and MgO-doped HAp were prepared via combined hydrothermal base-acid wet and co-precipitation techniques. The preparation involves the use of eggshell waste as the biosources material and MgO metal filler as the dopant of the same particle size (90 µm) to form the composite.

The material formation implied the simultaneous hydrothermal calcination and base-acid wet technique were appropriate for the synthesis of HAp and MgO-doped HAp,

and the complete elimination of organic matter from the unprocessed eggshell powder with good material yield. From the study's results, the HAp and MgO-doped HAp samples have phase, chemical, and bioactivity properties comparable to the biomaterial found in calcified human bones. The addition of MgO fillers had significantly impacted the doped HAp sample and its characteristics. Physiochemical, crystallographic, thermal, antimicrobial, and morphological properties have shown that this material has improved the properties of HAp with good thermal stability.

Notably, eggshells are natural composites comprising mainly of HAp, that is, a type of calcium phosphate with a chemical architecture that is essentially identical to that of natural bones. This study encourages the use of natural resources and the mitigation of significant health and environmental hazards related to eggshell waste in the agro-food sector. The results of this study demonstrate that HAp and MgO-doped HAp composites can be developed into an industrially feasible and sustainable option for bone tissue regeneration.

## AUTHOR CONTRIBUTIONS

**A. O. Ogunsanya:** Involved in conceptualization, supervision, data curation, editing, and reviewing of the draft, and was a major contributor to writing the manuscript. **E. O. Makinde, A. F. Aba & K. A. Lawal:** Involved in conceptualization, data curation, and editing and reviewing of the draft. **D. O. Daramola, A. T. Olabinjo & O. E. Ogundoyin:** Involved in conceptualization, supervision, article draft review, and revision. All authors read and approved the final manuscript.

## REFERENCES

- Achar, T. K., A. Bose and P. Mal (2017).** Mechanochemical synthesis of small organic molecules. *Beilstein Journal of Organic Chemistry*, 13, 1907–1931. <https://doi.org/10.3762/bjoc.13.186>
- Akindoyo, J. O.; S. Ghazali; M. D. H. Beg and N. Jeyaratnam (2019).** Characterization and Elemental Quantification of Natural Hydroxyapatite Produced from Cow Bone. *Chemical Engineering & Technology*, 42(9), 1805–1815. <https://doi.org/10.1002/ceat.201800636>
- Alanis-Gómez, R. P.; F. Hernández-Rosas; J. D.; Olivares-Hernández; E. M. Rivera-Muñoz; A. Zapatero-Gutiérrez; N. Méndez-Lozano; J. R. Alanis-Gómez and R. Velázquez-Castillo (2024).** Magnesium-Doped Hydroxyapatite Nanofibers for Medicine Applications: Characterization, Antimicrobial Activity, and Cytotoxicity Study. *International Journal of Molecular Sciences*, 25(22), 12418. <https://doi.org/10.3390/ijms252212418>.
- Alonzo, M.; F. A. Primo; S. A. Kumar; J. A. Mudloff; E. Dominguez; G. Fregoso; N. Ortiz; W. M. Weiss and B. Joddar (2021).** Bone tissue engineering techniques, advances, and scaffolds for treatment of bone defects. *Current Opinion in Biomedical Engineering*, 17, 100248.
- Asadipour, K.; N. Nezafati; M. S. Nourbakhsh; M. Hafezi-Ardakani and S. Bohloli (2019).** Characterization

and biological properties of a novel synthesized silicon-substituted hydroxyapatite derived from eggshell. *The International Journal of Artificial Organs*, 42(2), 95–108. <https://doi.org/10.1177/0391398818806159>

**Asmawati, A. (2017).** Identification of inorganic compounds in eggshells as a dental remineralization material. *Journal of Dentomaxillofacial Science*, 2(3), 168. <https://doi.org/10.15562/jdmfs.v2i3.622>

**Bakr, A.; B. Anis and W. El Hotaby (2022).** Sounchemical synthesis of Graphene/nano-hydroxyapatite composites for potential biomedical application. *Egyptian Journal of Chemistry*, 65(2), 669–678. <https://doi.org/10.21608/ejchem.2021.91241.4339>

**Bhatnagar, D.; S. Gautam; L. Sonowal; S. S. Bhinder; S. Ghosh and F. Pati (2024).** Enhancing Bone Implants: Magnesium-Doped Hydroxyapatite for Stronger, Bioactive, and Biocompatible Applications. *ACS Applied Bio Materials*, 7(4), 2272–2282. <https://doi.org/10.1021/acsabm.3c01269>

**Bulina, N. V.; N. V. Eremina; S. V. Makarova; I. A. Borodulina; O. B. Vinokurova; L. A. Avakyan; E. V. Paramonova; V. S. Bystrov and O. A. Logutenko (2024).** Influence of Magnesium Source on the Mechanochemical Synthesis of Magnesium-Substituted Hydroxyapatite. *Materials*, 17(2), Article 2. <https://doi.org/10.3390/ma17020416>

**Canbay, C. A.; H. I. Mustafa and İ. Özkul (2018).** Characterization of Hydrothermally Synthesised Hydroxyapatite Bioceramic. *Turkish Journal of Engineering*, 2(1), 1–6. <https://doi.org/10.31127/tuje.327822>

**Ciosek, Ż.; K. Kot; D. Kosik-Bogacka; N. Łanocha-Arendarczyk and I. Rotter (2021).** The Effects of Calcium, Magnesium, Phosphorus, Fluoride, and Lead on Bone Tissue. *Biomolecules*, 11(4), 506.

**Das Lala, S.; E. Barua; P. Deb and A. B. Deoghare (2021).** Physico-chemical and biological behaviour of eggshell bio-waste derived nano-hydroxyapatite matured at different aging time. *Materials Today Communications*, 27, 102443. <https://doi.org/10.1016/j.mtcomm.2021.102443>.

**Dauda, K. T.; C. A. Majebi; A. A. Ayoola; O. Agboola; A. P. I. Popoola; O. S. L. Fayomi; S. O. Banjo; J. Sojobi and A. O. Ogunsanya (2021).** Biosmart Materials and Its Innovative Characteristics in Protective Composite Coating Application. *IOP Conference Series: Materials Science and Engineering*, 1107(1), 012216

**Dec, P.; A. Modrzejewski and A. Pawlik, A. (2022).** Existing and Novel Biomaterials for Bone Tissue Engineering. *International Journal of Molecular Sciences*, 24(1), 529.

**Ebrahimi, S.; C. Stephen Sipaut@ Mohd Nasri and S. E. Bin Arshad (2021).** Hydrothermal synthesis of hydroxyapatite powders using Response Surface Methodology (RSM). *PLoS ONE*, 16(5), e0251009.

**Elmaazouzi, L.; B. Lizoul; A. Driouch; M. Lechheb; O. Dagdag; I. Lmachraa; S. Tayoub; A. Jaafar and Z. Lakbaibi (2024).** Potential of Moroccan Discarded Sardine: An Assessment Approach for Advancing Circular Economy Practices. In A. Thakur & A. Kumar (Eds.), *Advances in Chemical and Materials Engineering* (pp. 186–245). IGI Global.

**Etinosa, P. O.; O. A. Osuchukwu; E. O. Anisiji; M. Y. Lawal; S. A. Mohammed; O. L. Ibitoye; P. G. Oni; V. D. Aderibigbe; T. Aina; D. Oyeboode and S. C. Nwigbo (2024).** In-depth review of synthesis of hydroxyapatite biomaterials from natural resources and chemical reagents for biomedical applications. *Arabian Journal of Chemistry*, 17(12), 106010. <https://doi.org/10.1016/j.arabjc.2024.106010>.

**George Ittycheria, P.; T. George; M. John; G. Meenu; V. Thomas; S. Aswathy; R. Kuriakose and J. Thomas (2024).** Application of Hydroxyapatite in Regenerative Dentistry. In P. Vitureanu & M. Simona Baltatu (Eds.), *Biomedical Engineering* (Vol. 23). IntechOpen.

**Goyal, V.; G. C. Verma and P. Saxena (2024).** Advancements in 3D printing of functional materials for biomedical applications: Challenges, opportunities, and case studies: a critical review. *Progress in Additive Manufacturing*. <https://doi.org/10.1007/s40964-024-00901-9>

**Haghshenas, M. (2017).** Mechanical characteristics of biodegradable magnesium matrix composites: A review. *Journal of Magnesium and Alloys*, 5(2), 189–201.

**Horta, M. K. D. S.; F. J. Moura; M. S. Aguilar; C. B. Westin; D. Navarro Da Rocha and J. B. De Campos (2021).** *In vitro* evaluation of natural hydroxyapatite from *Osteoglossum bicirrhosum* fish scales for biomedical application. *International Journal of Applied Ceramic Technology*, 18(6), 1930–1937.

**Hung, C. C.; A. Chaya; K. Liu; K. Verdelis and C. Sfeir (2019).** The role of magnesium ions in bone regeneration involves the canonical Wnt signaling pathway. *Acta Biomaterialia*, 98, 246–255.

**Irfan, Md.; P. S. Suprajaa; R. Praveen and B. M. Reddy (2021).** Microwave-assisted one-step synthesis of nanohydroxyapatite from fish bones and mussel shells. *Materials Letters*, 282, 128685.

**Jenifer, A.; K. Senthilarasan; S. Arumugam; P. Sivaprakash; S. Sagadevan and P. Sakthivel (2021).** Investigation on antibacterial and hemolytic properties of magnesium-doped hydroxyapatite nanocomposite. *Chemical Physics Letters*, 771, 138539.

**Karacabey, P.; S. Döven; D. Uzunoğlu and A. Özer (2019).** Synthesis of 3D Hierarchical Flower-like MgO Microstructure: Investigation of its Adsorption and Antibacterial Properties. *Arabian Journal for Science and Engineering*, 44(12), 9951–9964.

**Karunakaran, G.; E. B. Cho; G. S. Kumar; E. Kolesnikov; G. Janarthanan; M. M. Pillai; S. Rajendran; S. Boobalan; K. G. Sudha and M. P. Rajeshkumar (2020).** Mesoporous Mg-doped hydroxyapatite nanorods prepared from bio-waste blue mussel shells for implant applications. *Ceramics International*, 46(18, Part A), 28514–28527.

**Krishani, M.; W. Y. Shin; H. Suhaimi and N. S. Sambudi (2023).** Development of Scaffolds from Bio-Based Natural Materials for Tissue Regeneration Applications: A Review. *Gels*, 9(2), 100.

**Lee, S. S.; X. Du; I. Kim and S. J. Ferguson (2022).** Scaffolds for bone tissue engineering. *Matter*, 5(9), 2722–2759.

**Liu, Y.; Y. Tang; J. Wu; J. Sun; X. Liao; Z. Teng and G. Lu (2020).** Facile synthesis of biodegradable flower-like

hydroxyapatite for drug and gene delivery. *Journal of Colloid and Interface Science*, 570, 402–410.

**Mahanty, A. and Shikha, D. (2021).** Calcium substituted with magnesium, silver and zinc in hydroxyapatite: A review. *International Journal of Materials Research*, 112(11), 922–930.

**Mahanty, A. and Shikha, D. (2024).** Design of a new Ag/Mg/Zn alloyed doped hydroxyapatite hybrid biomaterial. *Materials Chemistry and Physics*, 311, 128553. <https://doi.org/10.1016/j.matchemphys.2023.128553>.

**Mohd Pu'ad, N. A. S.; R. H. Abdul Haq; H. Mohd Noh; H. Z. Abdullah; M. I. Idris and T. C. Lee (2020).** Synthesis method of hydroxyapatite: A review. *Materials Today: Proceedings*, 29, 233–239.

**Monte, J. P.; A. Fontes; G. A. L. Pereira; G. Pereira and B. S. Santos (2022).** Preparation and characterization of Mg(II) doped hydroxyapatite biocomposites. *Results in Chemistry*, 4, 100625.

**Mustafa, W.; U. Azhar; S. Tabassum; M. Jamal; S. A. Siddiqi; M. Tariq; N. Muhammad; A. Asif; A. A. Chaudhry and F. Sharif (2020).** Doping and Incorporation of Hydroxyapatite in Development of PU-PLA Electrospun Osteogenic Membranes. *Journal of Polymers and the Environment*, 28(11), 2988–3002.

**Obada, D. O.; K. A. Salami; A. N. Oyediji; O. O. Fasanya; M. U. Suleiman; B. A. Ibisola; A. Y. Atta; D. Dodoo-Arhin; L. S. Kuburi; M. Dauda and E. T. Dauda (2021).** Solution combustion synthesis of strontium-doped hydroxyapatite: Effect of sintering and low compaction pressure on the mechanical properties and physiological stability. *Materials Letters*, 304, 130613. <https://doi.org/10.1016/j.matlet.2021.130613>.

**Ogunsanya, A. O.; E. B. Iorohol; D. Arinze and O. Ogundoyin (2024).** Evaluation of MgO-ZnO-Crab Shell Biofillers as Reinforcement for Biodegradable Poly(lactic Acid) (PLA) Composite. *Nigerian Journal of Technological Development*, 21(2), 10–21.

**Osuchukwu, O. A.; A. Salihi; I. Abdullahi; P. O. Etinosa and D. O. Obada (2023).** A comparative study of the mechanical properties of sol-gel derived hydroxyapatite produced from a novel mixture of two natural biowastes for biomedical applications. *Materials Chemistry and Physics*, 297, 127434.

**Osuchukwu, O. A.; A. alih; T. Abdullahi and D. O. Obada (2022a).** Taguchi grey relational optimization of sol-gel derived hydroxyapatite from a novel mix of two natural biowastes for biomedical applications. *Scientific Reports*, 12(1), 17968.

**Osuchukwu, O. A.; A. Salihi; I. Abdullahi; D. O. Obada; S. A. Abolade; A. Akande and S. Csaki (2022b).** Structural and nano-mechanical characteristics of a novel mixture of natural hydroxyapatite materials: Insights from ab-initio calculations and experiments. *Materials Letters*, 326, 132977.

**Panda, S.; C. K. Biswas and S. Paul (2021).** A comprehensive review on the preparation and application of calcium hydroxyapatite: A special focus on atomic doping methods for bone tissue engineering. *Ceramics International*, 47(20), 28122–28144.

**Perić Kačarević, Ž.; P. Rider; S. Alkildani; S. Retnasingh; M. Pejakić; R. Schettler; M. Gosau; R. Smeets; Q. Jung and M. Barbeck (2020).** An introduction to bone tissue engineering. *The International Journal of Artificial Organs*, 43(2), 69–86. <https://doi.org/10.1177/0391398819876286>.

**Predoi, D.; S. C. Ciobanu; S. L. Iconaru and M. V. Predoi (2023).** Influence of the Biological Medium on the Properties of Magnesium Doped Hydroxyapatite Composite Coatings. *Coatings*, 13(2), 409.

**Predoi, D.; S. L. Iconaru; M. V. Predoi; M. Motelica-Heino; N. Buton and C. Megier (2020).** Obtaining and Characterizing Thin Layers of Magnesium Doped Hydroxyapatite by Dip Coating Procedure. *Coatings*, 10(6), 510.

**Predoi, D.; S. L. Iconaru; M. V. Predoi; G. E. Stan and N. Buton (2019).** Synthesis, Characterization, and Antimicrobial Activity of Magnesium-Doped Hydroxyapatite Suspensions. *Nanomaterials*, 9(9), 1295.

**Pu'ad, N. M.; R. A. Haq; H. M. Noh; H. Z. Abdullah; M. I. Idris and T. C. Lee (2020).** Synthesis method of hydroxyapatite: A review. *Materials Today: Proceedings*, 29, 233–239.

Qu, H., Fu, H., Han, Z., & Sun, Y. (2019). Biomaterials for bone tissue engineering scaffolds: A review. *RSC Advances*, 9(45), 26252–26262.

**Raafat, A. I.; H. Kamal; H. M. Sharada; S. A. Abd Elhalim and R. D. Mohamed (2020).** Radiation Synthesis of Magnesium Doped Nano Hydroxyapatite/(Acacia-Gelatin) Scaffold for Bone Tissue Regeneration: In Vitro Drug Release Study. *Journal of Inorganic and Organometallic Polymers and Materials*, 30(8), 2890–2906.

**Radulescu, D. E.; O. R. Vasile; E. Andronescu and A. Fikai (2023).** Latest Research of Doped Hydroxyapatite for Bone Tissue Engineering. *International Journal of Molecular Sciences*, 24(17), 13157.

**Raveendran, S.; Y. Yoshida; T. Maekawa and D. S. Kumar (2013).** Pharmaceutically versatile sulfated polysaccharide based bionano platforms. *Nanomedicine: Nanotechnology, Biology and Medicine*, 9(5), 605–626.

**Sahmani, S., S. Saber-Samandari; A. Khandan and M. Mohammadi Aghdam (2019).** Influence of MgO nanoparticles on the mechanical properties of coated hydroxyapatite nanocomposite scaffolds produced via space holder technique: Fabrication, characterization and simulation. 95, 76–88.

**Sohn, H. S. and Oh, J. K. (2019).** Review of bone graft and bone substitutes with an emphasis on fracture surgeries. *Biomaterials Research*, 23(1), 1–7.

**Stella, S. M., T. M. Sridhar; R. Ramprasath; J. Gimbin and U. Vijayalakshmi (2022).** Physio-Chemical and Biological Characterization of Novel HPC (Hydroxypropylcellulose): HAP (Hydroxyapatite):PLA (Poly Lactic Acid) Electrospun Nanofibers as Implantable Material for Bone Regenerative Application. *Polymers*, 15(1), 155.

**Szterner, P. and Biernat, M. (2022).** The Synthesis of Hydroxyapatite by Hydrothermal Process with Calcium Lactate Pentahydrate: The Effect of Reagent Concentrations,

pH, Temperature, and Pressure. *Bioinorganic Chemistry and Applications*, 2022(1), 3481677.

**Waheed, S., M. Sultan; T. Jamil and T. Hussain (2015).** Comparative Analysis of Hydroxyapatite Synthesized by Sol-gel, Ultrasonication and Microwave Assisted Technique. *Materials Today: Proceedings*, 2(10, Part B), 5477–5484.

**Walmsley, G. G.; R. C. Ransom; E. R. Zielins; T. Leavitt; J. S. Flacco; M. S. Hu; A. S. Lee; M. T. Longaker and D. C. Wan (2016).** Stem Cells in Bone Regeneration. *Stem Cell Reviews and Reports*, 12(5), 524–529.

**Yelten-Yilmaz, A. and Yilmaz, S. (2018).** Wet chemical precipitation synthesis of hydroxyapatite (HA) powders. *Ceramics International*, 44(8), 9703–9710.

**Zhang, L. Y.; Q. Bi; C. Zhao; J. Y. Chen; M. H. Cai and X. Y. Chen (2020).** Recent advances in biomaterials for the treatment of bone defects. *Organogenesis*, 16(4), 113–125.

**Zhang, K.; Y. Liu; Z. Zhao; X. Shi; R. Zhang; Y. He; H. Zhang; Y. Sun and W. Wang (2023).** Synthesis Technology of Magnesium-Doped Nanometer Hydroxyapatite: A Review. *ACS Omega*, 8(47), 44458–44471. <https://doi.org/10.1021/acsomega.3c06091>